frontiers in Earth Science

ORIGINAL RESEARCH
published: 09 April 2021
doi: 10.3389/feart.2021.615766

Insight Into Hartoušov Mofette, Czech Republic: Tales by the Fluids

Kyriaki Daskalopoulou[1], Heiko Woith[1], Martin Zimmer[1], Samuel Niedermann[1], Johannes A. C. Barth[2], Alexander H. Frank[2], Andrea Vieth-Hillebrand[1], Josef Vlček[3], Cemile Dilara Bağ[1,4] and Ralf Bauz[1]*

[1] GFZ German Centre for Geosciences, Potsdam, Germany, [2] GeoZentrum Nordbayern, Schlossgarten 5, Department Geographie und Geowissenschaften, Friedrich-Alexander-Universität Erlangen-Nürnberg, Nürnberg, Germany, [3] Department of Hydrogeology, Engineering Geology and Applied Geophysics, Faculty of Science, Charles University, Prague, Czechia, [4] Department of Geological Engineering, Middle East Technical University, Ankara, Turkey

The Cheb Basin (Czech Republic) is characterized by emanations of magma-derived gases and repeated occurrences of mid-crustal earthquake swarms with small to intermediate magnitudes ($M_L < 4.5$). Associated intense mantle degassing occurs at the Hartoušov Mofette, a representative site for the Cheb Basin. Here, we performed 14 sampling campaigns between June 2019 and March 2020. Gas samples of fluids ascending in two boreholes (F1, ∼28 m depth and F2, ∼108 m depth) and from a nearby natural mofette were analyzed for their chemical (CO_2, N_2, O_2, Ar, He, CH_4, and H_2) and isotope compositions (noble gases and CO_2). CO_2 concentrations were above 99.1% in most samples, while O_2 and N_2 were below 0.6%. He ranged from 19 to 34 μmol/mol and CH_4 was mostly below 12 μmol/mol. Isotope compositions of helium and carbon in CO_2 ranged from 5.39 to 5.86 R_A and from −2.4 to −1.3 ‰ versus VPDB, respectively. Solubility differences of the investigated gases resulted in fluctuations of their chemical compositions. These differences were accompanied by observed changes of gas fluxes in the field and at the monitoring station for F1. Variations in solubilities and fluxes also impacted the chemical concentration of the gases and the $\delta^{13}C$ values that were also likely influenced by Fischer-Tropsch type reactions. The combination of (a) the Bernard ratio, (b) $CH_4/^3He$ distributions, (c) P-T conditions, (d) heat flow, and (e) the sedimentary regime led to the hypothesis that CH_4 may be of mixed biogenic and volcanic/geothermal origin with a noticeable atmospheric contribution. The drilling of a third borehole (F3) with a depth of ∼238 m in August 2019 has been crucial for providing insights into the complex system of Hartoušov Mofette.

Keywords: geogenic degassing, CO_2-rich fluids, solubility, CH_4 origin, gas flow perturbations

OPEN ACCESS

Edited by:
Yunpeng Wang,
Guangzhou Institute of Geochemistry, Chinese Academy of Sciences, China

Reviewed by:
Xianrong Zhang,
Qingdao Institute of Marine Geology(QIMG), China
Galip Yuce,
Hacettepe University, Turkey

****Correspondence:***
Kyriaki Daskalopoulou
kyriaki.daskalopoulou@gfz-potsdam.de;
kikdaskalopoulou@gmail.com

Specialty section:
This article was submitted to Geochemistry, a section of the journal Frontiers in Earth Science

Received: *09 October 2020*
Accepted: *03 March 2021*
Published: *09 April 2021*

Citation:
Daskalopoulou K, Woith H, Zimmer M, Niedermann S, Barth JAC, Frank AH, Vieth-Hillebrand A, Vlček J, Bağ CD and Bauz R (2021) Insight Into Hartoušov Mofette, Czech Republic: Tales by the Fluids. Front. Earth Sci. 9:615766. doi: 10.3389/feart.2021.615766

INTRODUCTION

Gases from various tectonic regions can differ in their geochemical characteristics (Lupton, 1983). Therefore, detailed studies of geothermal gases often contribute to an improved understanding of tectonic and geological settings and their corresponding fluids (Giggenbach, 1992, 1996; Lee et al., 2005). Furthermore, geodynamic settings are often influenced by seismic, volcanic, and geothermal activities and that also plays an essential role in earth degassing (Irwin and Barnes, 1980).

Hydrothermal fluids transport volatiles from the deep crust or mantle to the surface, while their circulation in the crust can also enhance geodynamic processes. The generation and transportation of these fluids are linked to a plethora of faulting processes (including nucleation, propagation, arrest, and recurrence of earthquake ruptures, fault creep or slow earthquakes, and the long-term structural and compositional evolution of fault zones – Hickman et al., 1995). Their study therefore offers a tool for monitoring and better understanding mantle and crustal processes.

Geogenic CO_2 discharges are widespread throughout central Europe (Pearce et al., 2004). Although they occur in diverse geological and geodynamic settings their distribution is principally controlled by the Cenozoic rift systems and associated Tertiary volcanism. The Eger Rift (Czech Republic, **Figure 1A**) is an intraplate region without active volcanism (youngest volcanic activity took place 0.29 Ma ago- Mrlina et al., 2009). However, emanations of magma-derived gases take place in the western part of the Cheb Basin (Weinlich et al., 1999; Geissler et al., 2005). This area associates with earthquake swarms that are likely induced by the ascent of the magmatic fluids (Parotidis et al., 2003). Variations in the gas flow together with chemical and isotope compositions were noticed during periods of seismic activity (Bräuer et al., 2018). For instance, increase in the gas flow was observed at the Hartoušov mofette field (HMF) after a series of earthquakes in 2014 (Fischer et al., 2017). During the same period, the gas flow in the mofette field of Dolní Částkov (Cheb Basin) decreased drastically. Post-seismic shifts in $\delta^{13}C_{CO2}$ and $^{3}He/^{4}He$ after the small swarm on the 4th and 5th of December 1994 were documented by Weise et al. (2001). They estimated the fluid transport velocities in the upper crust at 400 m/d for the Bublák mofette field. Spatial and temporal increase of mantle-derived helium contributions in the eastern Cheb Basin suggested that fluid injection channels reach down to the lithospheric mantle (Bräuer et al., 2005, 2009). It is worth noting that the subcontinental lithospheric mantle (SCLM) contribution at HMF increased from 38% in 1993 to 89% in 2016 (Bräuer et al., 2018), while the isotope ratio of He at the Bublák mofette reached 6.3 R_A before the earthquake swarms in 2000 and 2008. This increase indicated that ascending magma from the SCLM into the crust might have triggered the swarm.

These observations highlight the complexity and uniqueness of the Cheb Basin, and illustrate the need to deepen our knowledge on the system. Especially the relationship between the fluids and the seismic activity demands further research. Toward this goal, this investigation focuses on monitoring fluids encountered at different depths of the HMF (**Figure 1B**). Gases emerging in the mofette (surface expression), as well as in two boreholes (F1 and F2 with depths ∼28 m ∼108 m, respectively) have been sampled regularly over 1 year. Our study aims to identify key processes affecting the gases in the *"micro"*-system of HMF. We also aimed to show first results of gases during the drilling period of a third borehole. This was drilled during the study period, to a depth of ∼238 m. Moreover, our study takes a first step toward the determination of the origin of CH_4.

This work is part of the Mofette Research (MoRe) project, which combines geochemical and geophysical methods to document how fluids can actively act in a non-volcanic rift setting of intraplate seismicity.

STUDY AREA

The Cheb Basin is an asymmetric intracontinental basin that lies within the western part of the Eger Rift close to the Nový Kostel focal zone (NK, Fischer and Horálek, 2003; **Figure 1**). In its eastern part, the basin is defined by the NNW-SSE Mariánské Lázně Fault Zone (MLFZ). Its petrological regime includes rock sequences of Upper Cambrian to Ordovician age and areas characterized by Late Variscan intrusions that are dominated by granites. Its crystalline basement consists of muscovite granites of the Smrčiny/Fichtelgebirge Pluton (Hecht et al., 1997). These combine with crystalline schists of the Saxothuringian Zone of the Variscan Orogen (Fiala and Vejnar, 2004). The basin was formed during the Late Tertiary and Quaternary by the re-activation of Hercynian faults and separated microplates present within the basement (Bankwitz et al., 2003; Babuška and Plomerová, 2008) or either of them. The Cheb Basin was filled with 300 m-thick fluvial and lacustrine deposits (Špičáková et al., 2000; Nickschick et al., 2015). Volcanism in the western part of the Eger Rift was weak and of Quaternary age, and the youngest volcanic activity in the area took place 0.29 Ma ago (Mrlina et al., 2009).

Magma-derived volatiles present in the Cheb Basin consist of CO_2-rich waters, wells, and dry gas vents (Weinlich et al., 1999). The dominant gas species is CO_2 (>98%) with minor amounts of N_2, O_2, Ar, He, and CH_4 (Weinlich et al., 1999; Kämpf et al., 2013; Bräuer et al., 2018). Isotope compositions for both helium and carbon in CO_2 indicate a mantle origin of the fluids (Bräuer et al., 2018). Along with the emanation of magma-derived gases, the recurrence of swarms with small to intermediate magnitudes (M_L < 4.5) is characteristic for the area. Parotidis et al. (2003) hypothesized that the ascent of magmatic fluids triggers most of these anomalous earthquake activities. However, Fischer et al. (2014) suggested that fluids are probably not the only triggering factor of the swarms. It is worth noting that the lack of CO_2 emanations in the epicentral area of the Nový Kostel (NK) focal zone likely results from an impermeable rock formation above the fault zone (Bräuer et al., 2009). Nonetheless, it has produced almost 80% of the earthquake swarms during the past 30 years (Fischer and Michálek, 2008).

In order to investigate relationships between geodynamic processes, CO_2 degassing, and the continental "deep biosphere," three boreholes were drilled in the intensively degassing HMF (Dahm et al., 2013, 26 t/d of diffuse soil degassing; Kämpf et al., 2019). F1 [corresponding to 1H-031 in Bräuer et al. (2018) and VP8303 in Fischer et al. (2020)] was drilled in 2007 down to ∼28 m below ground and taps into a CO_2-saturated, confined aquifer. The F2 borehole [HJB-1 in Bräuer et al. (2018)] has a depth of ∼108 m, and was drilled in spring 2016 to investigate whether the increased fluid and substrate flow can accelerate microbial life in active fault zones

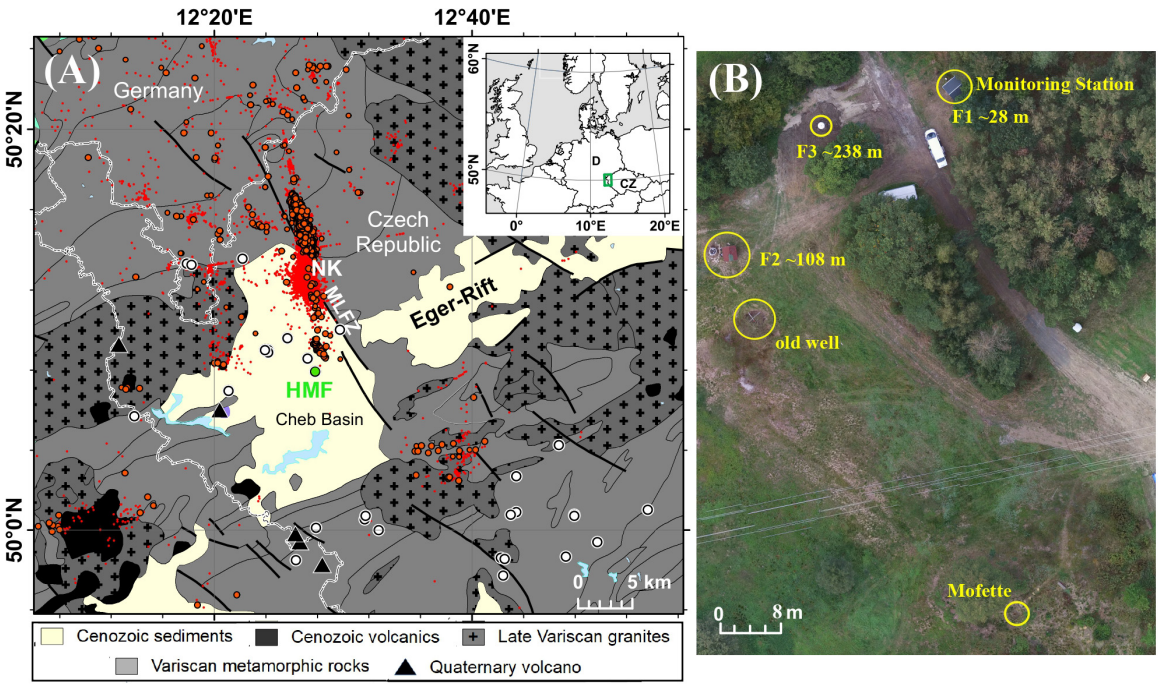

FIGURE 1 | (A) Simplified geological map of the Eger Rift area and its surroundings ["Geological Map of Germany 1:1 000 000 (GK1000)," BGR]. The Hartoušov Mofette Field (HMF) is indicated with a green circle. The white circles correspond to mofettes and springs with CO_2 gas flux >400 l/h, while the red circles portray the seismic activity during the past 30 years. The Mariánské Lázně Fault Zone (MLFZ), as well as the Nový Kostel focal zone (NK), are also shown. **(B)** Orthomosaic image of the HMF, where the positions of the 3 boreholes (F1, F2, and F3) along with their depths, the mofette, and the old well are indicated. A seismological and geochemical monitoring station located at F1 is also marked on the map.

and CO_2 conduits (Bussert et al., 2017). In August 2019, a third borehole (F3) was drilled to a depth of ~238 m. Its principal aim is to investigate the relation between geogenic degassing and earthquake activity by combination of geochemical and geophysical techniques. Further details about the borehole configuration can be found in Woith et al. (2020).

MATERIALS AND METHODS

From June 2019 to March 2020, 14 sampling campaigns took place in the HMF, and 40 gas samples were collected. Samples were obtained from the free gas phase after passage through water. They were collected in Exetainer vials and glass vessels with two vacuum stopcocks. The containers were first filled with water. Subsequently, gas was collected with tubing that was directly connected to the borehole head. Its upward flow replaced the water in the vessel. For mofette samples, the tubing was connected to an inverted funnel, which was immersed in the water. Three samples were collected per sampling site on each sampling day; one of these samples was used to determine the gas composition and the other two for noble gas and carbon isotope analyses of CO_2, respectively.

For analyses of their chemical composition, gases were sampled in 1,000 cm^3 glass vessels. The CO_2 contents were determined volumetrically after absorption in a KOH solution with a precision of 0.1 cm^3. The remaining CO_2-free aliquot was analyzed at a commercial laboratory in the Czech Republic (Labor Union) using gas chromatography. N_2 and O_2 had a relative precision of ± 3%, while the minor components (Ar, He, H_2, CH_4, and light hydrocarbons) were determined at relative precisions of ±10–40%. The detection limit for H_2 and He was <100 µmol/mol of CO_2-free gas, while for CH_4 and other light hydrocarbons it was <1 µmol/mol. This corresponded to 0.5 µmol/mol and 0.005 µmol/mol, respectively, in gas with CO_2 contents of 99.5%. Further details of the method are also available in Weinlich et al. (1998).

$\delta^{13}C$ analyses were performed from the Exetainer vials (12 cm^3) at GFZ Potsdam with a gas chromatograph (GC 6890N, Agilent Technologies, equipped with Plot column) coupled via a combustion device (GC-C/TC III, Thermo Fisher Scientific) to an isotope ratio mass spectrometer (MAT253, Thermo Fisher Scientific). The $\delta^{13}C$ values are reported in ‰ versus Vienna Pee Dee Belemnite (VPDB) standard with a standard deviation of ±0.3‰.

Samples for noble gas analyses were collected in 250 cm^3 glass vessels with two vacuum stopcocks. The isotopic composition of noble gases was determined for selected samples at GFZ Potsdam. For this purpose, aliquots were analyzed for noble gas concentrations and isotopic compositions with a VG 5400 noble gas mass spectrometer after removing the active gas components in a gas purification line. Details of the analytical procedure

can be found in Niedermann et al. (1997). The precision of He isotope measurements generally ranges from ±1.7% to ± 2.4%, with only four samples [(7), (18), (31), and (33)] being above this range (± 4.7% in average). The precision of $^4He/^{20}Ne$ generally ranges from ± 5.5% to ± 16% at 2σ (95% confidence) level. An exception to the latter range is sample (25) (± 84%), because of an extremely low Ne concentration. The measured $^3He/^4He$ ratios were corrected for atmospheric He contributions by assuming that contributions of ^{20}Ne are entirely of atmospheric origin, and by using the $^4He/^{20}Ne$ ratio of air (0.319) according to Craig et al. (1978):

$$(3/4)_c = \frac{[(3/4)_{sample} \times (4/20)_{sample}/(4/20)_{air} - (3/4)_{air}]}{[(4/20)_{sample}/(4/20)_{air} - 1]} \quad (1)$$

where 3/4 and 4/20 are the $^3He/^4He$ and $^4He/^{20}Ne$ ratios. Corrections were <3%, except for sample (1) (∼5%).

TABLE 1 | Analytical results of collected gas samples.

ID	Name	Date	Drilling Depth	CO_2	N_2	O_2	He	H_2	Ar	CH_4	C_2H_4	C_2H_6	C_3H_8
			m		%					μmol/mol			
1	F1	18.06.19		99.72	0.22	0.05	22.2	b.d.l.	46.9	22.8	b.d.l.	0.083	b.d.l.
2	F1	31.07.19		99.79	0.16	0.04	19.1	b.d.l.	37.0	2.38	b.d.l.	0.073	b.d.l.
3	F1	01.08.19	1.9	99.73	0.20	0.06	23.4	b.d.l.	47.5	2.50	b.d.l.	0.090	b.d.l.
4	F1	14.08.19	41.3	99.56	0.31	0.12	27.2	b.d.l.	71.9	8.47	b.d.l.	0.097	b.d.l.
5	F1_AC	23.08.19	70.9	98.70	0.86	0.41	22.6	b.d.l.	264	9.05	0.053	0.093	0.013
6	F1	25.08.19	125.3	99.67	0.27	0.05	25.3	b.d.l.	52.4	22.9	0.013	0.092	b.d.l.
7	F1_AC	29.08.19	197.3	93.23	5.27	1.42	6.81	b.d.l.	756	2.72	b.d.l.	b.d.l.	b.d.l.
8	F1	30.08.19	239.3	99.57	0.34	0.08	26.5	b.d.l.	70.9	2.42	b.d.l.	0.101	b.d.l.
9	F1	04.09.19		99.75	0.20	0.05	25.8	b.d.l.	43.9	4.95	b.d.l.	b.d.l.	b.d.l.
10	F1	06.09.19		99.47	0.39	0.13	26.8	b.d.l.	91	3.53	b.d.l.	b.d.l.	b.d.l.
11	F1	25.09.19		99.58	0.30	0.11	26.1	b.d.l.	69.3	2.61	b.d.l.	0.107	b.d.l.
12	F1	26.11.19		99.74	0.21	0.04	23.2	b.d.l.	40.5	1.74	b.d.l.	0.056	b.d.l.
13	F1	16.01.20		99.36	0.48	0.15	25.0	b.d.l.	93.1	1.41	b.d.l.	0.039	b.d.l.
14	F1	04.03.20		99.60	0.29	0.10	26.4	b.d.l.	59.5	2.66	b.d.l.	0.145	b.d.l.
15	F2_AC	18.06.19		92.45	5.87	1.60	7.6	b.d.l.	835	5.32	b.d.l.	b.d.l.	b.d.l.
16	F2	31.07.19		99.82	0.15	0.02	22.0	b.d.l.	37.6	4.94	b.d.l.	0.086	b.d.l.
17	F2	01.08.19	1.9	99.76	0.17	0.05	23.6	b.d.l.	204	4.64	b.d.l.	0.093	b.d.l.
18	F2	14.08.19	41.3	99.51	0.35	0.13	28.0	b.d.l.	78.7	8.57	b.d.l.	0.084	b.d.l.
19	F2	23.08.19	70.9	99.71	0.21	0.07	26.2	b.d.l.	48.1	2.46	b.d.l.	0.077	b.d.l.
20	F2	25.08.19	125.3	99.86	0.12	0.01	22.7	b.d.l.	26.0	3.76	b.d.l.	0.098	b.d.l.
21	F2	29.08.19	197.3	99.79	0.17	0.03	18.7	b.d.l.	31.4	4.31	b.d.l.	0.078	b.d.l.
22	F2	30.08.19	239.3	99.87	0.12	0.01	31.8	0.27	23.8	6.42	b.d.l.	0.032	b.d.l.
23	F2	03.09.19		99.87	0.11	0.02	24.9	b.d.l.	23.8	5.99	b.d.l.	0.015	b.d.l.
24	F2	25.09.19		99.71	0.22	0.07	24.2	b.d.l.	49.9	5.40	b.d.l.	0.044	b.d.l.
25	F2	26.11.19		99.72	0.23	0.04	33.5	b.d.l.	44.3	4.38	b.d.l.	0.039	b.d.l.
26	F2	15.01.20		99.15	0.56	0.27	28.9	b.d.l.	128	0.54	b.d.l.	0.060	b.d.l.
27	F2	04.03.20		99.63	0.26	0.10	26.4	b.d.l.	62.8	4.13	b.d.l.	0.071	0.030
28	Mofette_AC	18.06.19		98.81	0.91	0.26	43.1	b.d.l.	155	10.1	b.d.l.	0.238	b.d.l.
29	Mofette	31.07.19		99.73	0.20	0.06	23.3	b.d.l.	44.3	6.12	b.d.l.	0.070	b.d.l.
30	Mofette	14.08.19	41.3	99.70	0.22	0.06	24.7	b.d.l.	173	7.64	b.d.l.	0.085	b.d.l.
31	Mofette_AC	23.08.19	70.9	97.70	1.77	0.51	21.1	b.d.l.	250	5.50	b.d.l.	0.069	b.d.l.
32	Mofette	25.08.19	128.3	99.75	0.20	0.04	24.1	b.d.l.	47.0	4.19	b.d.l.	0.079	b.d.l.
33	Mofette_AC	29.08.19	197.3	96.85	2.46	0.64	6.6	b.d.l.	355	6.92	b.d.l.	b.d.l.	b.d.l.
34	Mofette	30.08.19	239.3	99.74	0.22	0.03	25.1	b.d.l.	45.9	6.23	b.d.l.	0.074	b.d.l.
35	Mofette	03.09.19		99.85	0.12	0.02	20.3	b.d.l.	28.1	5.53	b.d.l.	0.060	b.d.l.
36	Mofette	06.09.19		99.75	0.19	0.04	24.6	b.d.l.	46.7	9.02	b.d.l.	b.d.l.	b.d.l.
37	Mofette	25.09.19		99.76	0.19	0.04	29.4	b.d.l.	42.7	6.46	b.d.l.	0.130	b.d.l.
38	Mofette	26.11.19		99.80	0.16	0.03	26.1	b.d.l.	35.9	10.5	b.d.l.	0.075	b.d.l.
39	Mofette	15.01.20		99.73	0.20	0.06	27.7	b.d.l.	43.4	11.1	b.d.l.	0.054	b.d.l.
40	Mofette	04.03.20		99.64	0.26	0.09	29.0	b.d.l.	66.2	3.57	b.d.l.	0.081	b.d.l.

The coordinates of (a) F1 and F2 are 50° 7′ 58.8″ N and 12° 27′ 46.8″ E and (b) the Mofette are 50° 7′ 55.2″ N and 12° 27′ 50.4″ E.
b.d.l. = below detection limit.

RESULTS

Names, sampling dates, chemical concentrations, and isotope values for the collected samples are presented in **Tables 1–3**. **Supplementary Table 1** shows the drilling dates and the bottom depth of F3. The coordinates of the three sites are displayed in the footnote of **Table 1**. Literature data by Bräuer et al. (2018) were considered as background values, and used for comparison. It is worth mentioning that literature data from Weinlich et al. (1999) and Kämpf et al. (2013) were not used in our study, because they were influenced by seismic activity, and may result in misleading conclusions.

CO_2 concentrations exceeded 99 % in most samples, while O_2 and N_2 were mostly below 0.3 and 0.6%, respectively (**Table 1**). Six samples presented lower CO_2 contents (down to 92.5%), most likely due to air contamination during sampling that was manifested in elevated O_2 and N_2 concentrations (up to 1.6 and 5.9%, respectively). These samples are included and presented in the current study, however, they are given in gray color and are signed with "_AC," which stands for Air Contamination.

He in the uncontaminated samples ranged from 18 to 34 μmol/mol, whereas lower concentrations were found in samples with enhanced air component. Ar showed a wide range of concentrations (24 to 835 μmol/mol). Concentrations of CH_4 were generally lower than 12 μmol/mol, while enrichments up to 23 μmol/mol were found in F1 before drilling and during drilling at a core depth of ∼125 m. The lowest CH_4 value (0.5 μmol/mol) was found at F2 in the sample collected after the perforation of the F3 steel casing after the drilling period. H_2 was always below detection limit, apart from one sample collected from F2 when the drilling reached its final depth. C_2H_4 and C_3H_8 were almost always below detection limit apart from three borehole samples [(5) and (6) for C_2H_4 and (5) and (27) for C_3H_8]. C_2H_6 was present in concentrations lower than 0.24 μmol/mol.

Noble gases, as well as carbon isotopes, were measured only in selected samples. The isotope composition of He showed values between 5.37 and 5.86 R_A (where R_A is the atmospheric $^3He/^4He$ ratio of 1.39×10^{-6}). Corresponding $^4He/^{20}Ne$ ratios covered a wide range of values (5.2 to ∼19,000). The samples analyzed for $\delta^{13}C_{CO2}$ were in the range of −2.4 to −1.3‰ vs. VPDB.

Water temperature and gas flow in F1, the wellhead and bottom-hole pressure in F2, and meteorological data were obtained from the monitoring station located at F1 in the HMF (**Figure 1B**). These data were obtained from the CO_2 network (CarbonNet) of Charles University of Prague. Details are provided in the Section of Data Availability Statement.

TABLE 2 | Carbon isotope composition of CO_2.

ID	$\delta^{13}C_{CO2}$ vs. VPDB [‰]
4	−1.3
6	−1.4
9	−1.5
10	−1.9
16	−1.9
20	−1.5
21	−1.7
22	−1.8
23	−2.0
29	−1.8
32	−1.4
34	−1.7
35	−2.4
36	−1.6

DISCUSSION

Processes Affecting the Gases

CO_2 is the dominant gas component emerging from the HMF, with He isotopes and $\delta^{13}C_{CO2}$ showing a mantle origin (Kämpf et al., 2013; Bräuer et al., 2018). In **Figure 2A**, the atmospheric gas component (here represented by N_2) is plotted together with CO_2 and CH_4, which are characteristic of hydrothermal-type components (Giggenbach et al., 1993). This ternary plot aims to identify secondary processes, such as dissolution (Italiano et al., 2014a). As expected, N_2 concentrations are strongly enhanced in the air contaminated samples (gray-colored symbols). Borehole samples (13) and (26), collected after the perforation, as well as samples from F1 collected when F3 arrived at its final depth [(8)] and after the drilling process [(10), (11), and (14)] are also enriched in N_2. This suggests a CO_2 loss that was probably caused by dissolution processes. An increase in CH_4 content is found for two F1 samples [(1) and (6) – **Figure 2A**].

In the He-N_2-Ar ternary diagram (**Figure 2B** – after Giggenbach et al., 1983), the vast majority of the samples are distributed inside the triangle delimited by N_2/Ar ratios of air and air-saturated water (ASW), and the He apex. This distribution shows a two-component mixing relationship between mantle and atmospheric sources. Furthermore, most of the N_2/Ar ratios approach the value of 50 (**Table 1**), the typical value of air-saturated waters (Heaton and Vogel, 1981; Fischer et al., 1998). This suggests that N_2 originates from a mixture of shallow air-saturated fluids and deep circulating groundwaters. Samples (17) and (30), collected when the drilling of F3 arrived at ∼2 m and ∼41 m depth, respectively, revealed an excess of Ar for so far unknown reasons, while samples affected by atmospheric contamination plot close to the air and ASW points.

Enrichments of the geogenic components are evident in the binary plot of He/Ar versus N_2/O_2 (**Figure 3A**), with F2 presenting the most extreme values (**Table 1**). In most cases, samples of HMF have stable CH_4 and He contents (**Figure 3B**). As expected, the variability of CH_4 is somewhat higher in samples not affected by air contamination (**Figure 3B**). The higher He concentration in the F2 samples collected at the end [(22)] and after the F3 drilling [(25)] indicates a CO_2 loss. This loss may have been caused by the strong solubility contrast of these gases in aquatic environments (Reid et al., 1987). This may have been enhanced by the low and non-thermal temperatures of the HMF (up to 15°C for F1 and F2 and up to 20°C for the Mofette during the summer period). D'Alessandro et al. (2014) suggested that

TABLE 3 | Helium concentrations and $^3He/^4He$ and $^4He/^{20}Ne$ ratios from selected samples in the HMF.

ID	^4He	$^3He/^4He$	Error (2σ)	$^4He/^{20}Ne$	Error (2σ)	$(^3He/^4He)_c$	Error (2σ)
	μmol/mol	R_A				R_A	
1	14.9	5.53	±0.13	5.20	±0.37	5.83	±0.14
4	17.4	5.76	±0.09	203	±18	5.77	±0.09
7	17.3	5.77	±0.27	600	±56	5.77	±0.27
12	18.7	5.79	±0.11	725	±61	5.79	±0.11
15	17.9	5.65	±0.13	12.24	±0.67	5.77	±0.13
17	18.7	5.82	±0.10	1660	±260	5.82	±0.10
18	20.7	5.82	±0.28	664	±78	5.82	±0.28
20	16.8	5.71	±0.08	326	±25	5.71	±0.08
21	16.8	5.68	±0.12	116.1	±8.3	5.69	±0.12
22	15.7	5.62	±0.10	18.7	±1.3	5.70	±0.10
25	19.9	5.78	±0.10	19000	±16000	5.78	±0.10
28	18.0	5.68	±0.11	220	±15	5.69	±0.11
30	18.6	5.82	±0.11	690	±100	5.82	±0.11
31	18.3	5.86	±0.26	1040	±100	5.86	±0.26
32	16.5	5.57	±0.09	11.30	±0.80	5.70	±0.09
33	19.2	5.37	±0.26	68.8	±6.0	5.39	±0.26
34	17.3	5.69	±0.09	22.7	±1.6	5.76	±0.09
38	18.5	5.66	±0.10	18.8	±1.3	5.74	±0.10

$(^3He/^4He)_c$ is the air-corrected $^3He/^4He$ ratio (Craig et al., 1978).
^4He concentrations in this table were obtained by relating the He partial pressure determined by noble mass spectrometry to the total pressure in the gas vessel used for the noble gas analyses, assuming that the latter was equal to atmospheric pressure. 2σ uncertainties of these values are estimated at ∼10–15%.

such contrasts may result in strong enrichments in less soluble gases, when a gas mixture rises through unsaturated waters at depleted gas/water ratios.

Enrichment in He content was also noticed in the air-contaminated sample (28) (**Figure 3B** and **Table 1**). However, a different approach in calculating the He concentration yields a much lower value (**Table 3**). This suggests that this difference may result from an analytical problem during gas chromatography. Samples from F1 collected during the 1st campaign [(1)] and when F3 arrived at ∼125 m depth [(6)] exhibit enrichments in CH_4 (**Figure 3B**). This was likely caused by biogenic generation of the gas, a hypothesis promoted by the sedimentary formations (Daskalopoulou et al., 2018), and also supported by the depleted values of the atmospheric components (Goff and Janik, 2002; Easley et al., 2011). It should be noted that CH_4 content changes are common, as the gas can be involved in many production and consumption processes (Rolston et al., 1993). Another possible scenario that may apply to sample (1), collected in June 2019, is that CH_4 was accumulated at the wellhead for the period that the borehole was sealed and due to its low density, it was among the first gases to escape. Consumption by microbial or inorganic oxidation of the gas may explain the depletion in CH_4 that is noticed in the borehole gases collected after the perforation [(13) and (26)]. Indeed, N_2/O_2 ratios of these samples and also of samples (17) and (30) are similar to air. This indicates that the atmospheric component of meteoric water has been modified by redox reactions that took place either in the subsoil or in the aquifer (D'Alessandro et al., 2010).

Relation Between Fluid Parameters and CO_2

Mean bubble fraction and water temperature at F1 are presented in **Figure 4**, along with the wellhead pressure at F2 and the meteorological conditions in the HMF over the drilling period. The mean bubble fraction was calculated according to Fischer et al. (2020), who showed that in boreholes and narrow tube-like mofettes, gas bubble contents in a water-gas mixture can be quantified from the pressure difference over a fixed depth interval. The high gas/water ratio is expressed as an increase in the gas flow and the high bubble fraction. This may also

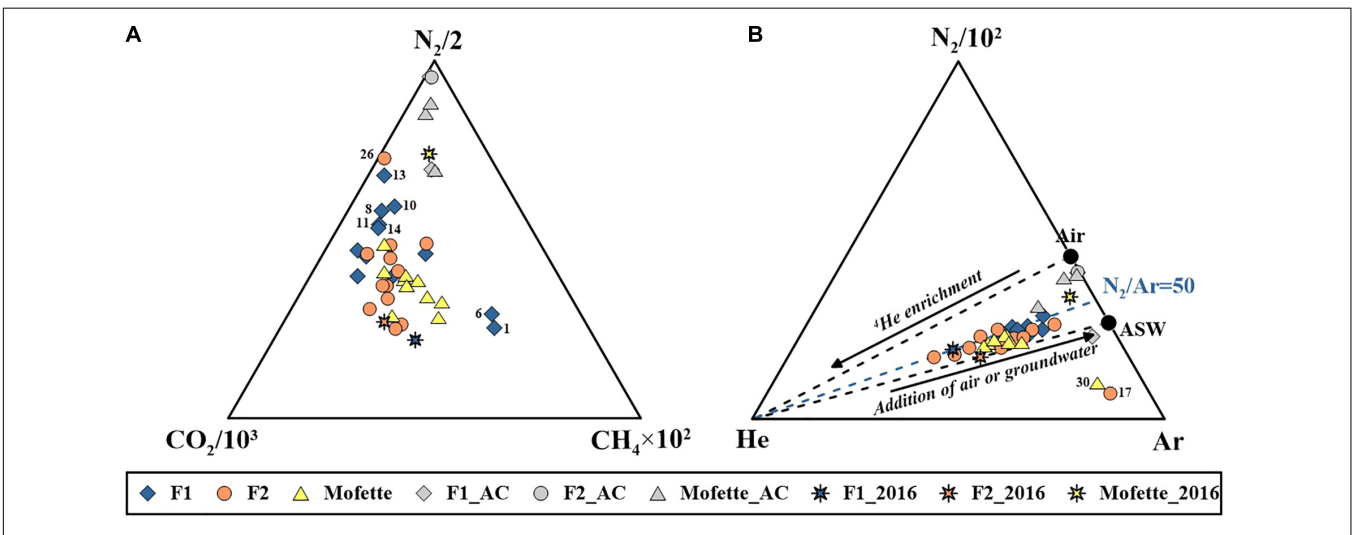

FIGURE 2 | (A) N_2-CO_2-CH_4 ternary diagram after Giggenbach et al. (1993) and **(B)** N_2-He-Ar ternary diagram after Giggenbach et al. (1983) of the gas emitted in the HMF. The abbreviation _AC stands for air contamination, while data of samples collected during 2016 are from Bräuer et al. (2018).

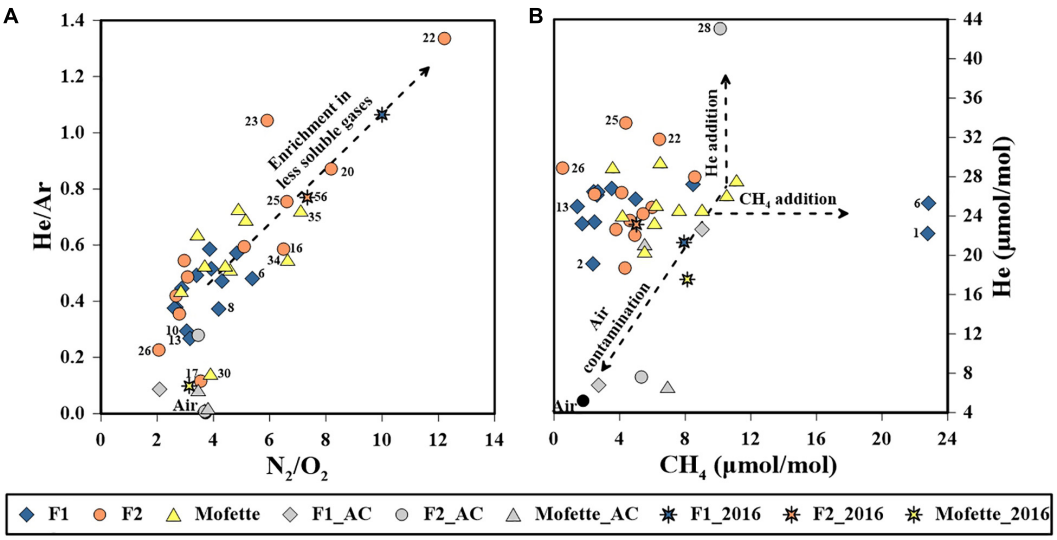

FIGURE 3 | Binary plots of **(A)** He/Ar vs. N_2/O_2 and **(B)** He vs. CH_4. Secondary processes are indicated with dashed arrows. The abbreviation _AC stands for air contamination, while data of samples collected during 2016 are from Bräuer et al. (2018).

cause higher $\delta^{13}C_{CO2}$ values as recognized in samples (4) and (6) (**Figure 5**). It might also be responsible for the depletion of the less soluble gases observed in samples (2) and (10) (**Figures 4A,D**).

Elevated gas flow and bubble fraction values in F1 correspond to depleted atmospheric components in the borehole and *vice versa* (**Figures 4A,D**). Provided that the concentration of atmospheric gases in the groundwater is constant, this observation indicates that mixing with a component of geogenic origin modifies the ratio. Moreover, low gas/water ratios (i.e., less intense bubbling) favor the dissolution, and hence the loss of CO_2 to the water (Reid et al., 1987). At the same time the limited ascent of geogenic gas can be contaminated more easily. The lack of gas flow and bubble fraction data at F2 and the mofette does not allow us to arrive at a similar conclusion for these locations.

Perturbations on the bubble fraction and the gas flow (F1) and on the wellhead pressure (F2) were observed when F3 was at a depth of ∼38 m (**Figure 4D**) and ∼110 m (**Figure 4B**), respectively. This indicates a hydraulic connection between the boreholes. This hypothesis was also supported by Woith et al. (2020), who documented a decrease in the gas flow and bubble fraction (**Figure 4D**) on the 30th of August. At the same time, the Rn concentration of the F3 drill mud reached its maximum. It is worth mentioning that a similar observation to the hydraulic connectivity, though on a larger scale, was made by Kämpf et al. (2013). They identified two connected conduit systems (Bublák and Hartoušov) that were interpreted as highly permeable substructures inside the Počatky–Plesná Fault Zone (PPZ). This observation was further studied by Nickschick et al. (2015), who hypothesized the existence of pull-apart basin-like structures inside the PPZ, and it was tested by Kämpf et al. (2019), who instead identified en-echelon faults, which act as fluid channels to depth.

Barometric pressures (note inverted scale in **Figure 4E**) are negatively correlated to the gas flow and bubble fraction at F1 (Woith et al., 2020). Fischer et al. (2020) explained this by proposing that elevated barometric pressures contribute to the dissolution of CO_2 that in turn hampers degassing. Even though the water temperature seems to be mostly constant, its perturbations are negatively correlated to the gas flow and bubble fraction (note inverted scale in **Figure 4C**). Despite its minor importance, it should be mentioned that the fractionation of C isotopes increases with decreasing temperature (Bottinga, 1968).

The relation between gases of different solubilities and $\delta^{13}C_{CO2}$ observed during the sampling period is presented in **Figure 5**. Gases collected when F3 reached a depth of ∼41 m [F1 (4)] and ∼125 m [F1 (6)] show a shift toward ^{13}C-enriched isotope values that may indicate fractionation due to preferential $^{12}C_{CO2}$ loss caused by phase separation. These phenomena have been observed for dissolved gases from the Apennines (Italy; Chiodini et al., 2000, 2013), the Southern Volcanic Zone of Chile (Ray et al., 2009), the Amik Basin (Turkey; Yuce et al., 2014), eastern Australia (Italiano et al., 2014b; Ring et al., 2016), and the Eastern Carpathians-Transylvanian Basin (Romania; Italiano et al., 2017). Moreover, the vigorous bubbling visible in the field and enhanced flow at F1 (Fischer et al., 2020; cf. **Figure 4**), suggest extensive degassing. This process promotes intense gas separation that subsequently causes isotope fractionation related to water-gas interactions.

Another possible explanation for elevated CH_4 contents and associated $\delta^{13}C_{CO2}$ values are Fischer-Tropsch type (FTT) reactions, during which gaseous CO_2 becomes reduced to produce abiogenic CH_4 (Berndt et al., 1996; Horita and Berndt, 1999; Foustoukos and Seyfried, 2004). Details on FTT reactions and abiogenic CH_4 are provided in the Section "Potential Origins of CH_4."

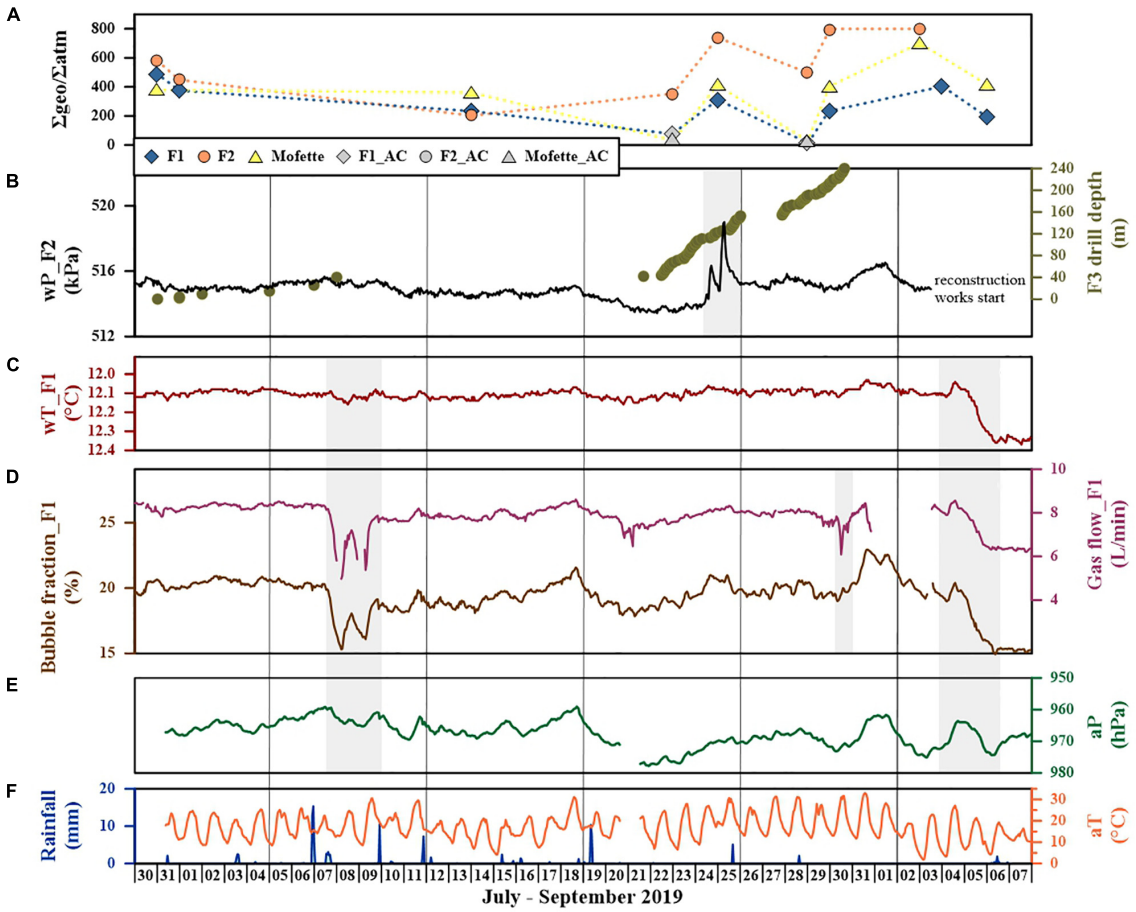

FIGURE 4 | Time series plot for the period 30th of July-7th of September 2019 showing **(A)** Σgeo/Σatm ratio in the two boreholes and the mofette, where Σgeo = CO_2+He+H_2+C_xH_y and Σatm = N_2+O_2+Ar, **(B)** the wellhead pressure (wP) of F2 and the drilling depth of F3 (Woith et al., 2020), **(C)** the water temperature (wT) in F1, **(D)** the calculated bubble fraction and the measured gas flow in F1, **(E)** the barometric pressure (aP) and **(F)** the meteorological conditions represented by the precipitation and the air temperature (aT). The axes of water temperature and barometric pressure are inverted. The vertical gray lines indicate the beginning of a new week, while the gray areas correspond to anomalies discussed in the text. Data of the gas flow and the temperature monitoring at Hartoušov are available at web.natur.cuni.cz/uhigug/carbonnet/en_index.html.

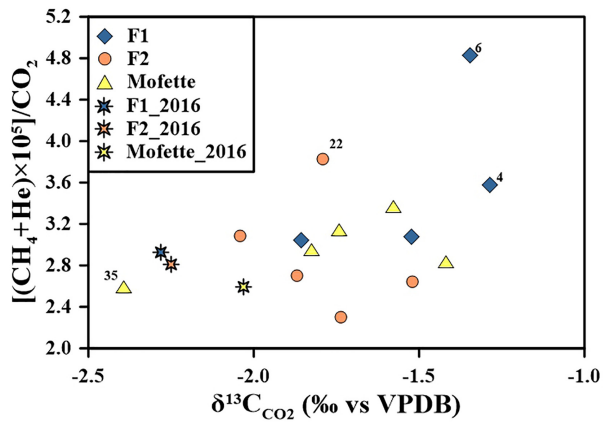

FIGURE 5 | Binary plot of (He+CH_4) /CO_2 vs. $\delta^{13}C_{CO2}$ for the gases of Hartoušov. Data of samples collected during 2016 are from Bräuer et al. (2018).

Sample (35) presents a shift toward more negative $\delta^{13}C$ values that may be related to a decrease in flow observed in the field. It should be also taken into consideration that the dissolution of CO_2 in the water results in CO_2 loss and lower $\delta^{13}C_{CO2}$ values. Moreover, if the hydraulic connection is real, then the mixing of gases ascending from different depths may have had an impact on the $\delta^{13}C$ and chemical composition. Overall the atmospheric components should decrease with increasing depth, while the geogenic components should increase. However, due to the limited amount of data and the standard deviation of the $\delta^{13}C_{CO2}$ values, no conclusions regarding the isotopic changes can be reached in the present work.

Potential Origins of CH_4

In geothermal and volcanic systems, the $CH_4/^3He$ ratio may differentiate possible methane sources (e.g., Welhan and Craig, 1983; Poreda et al., 1988); ^3He is mantle-derived, and the

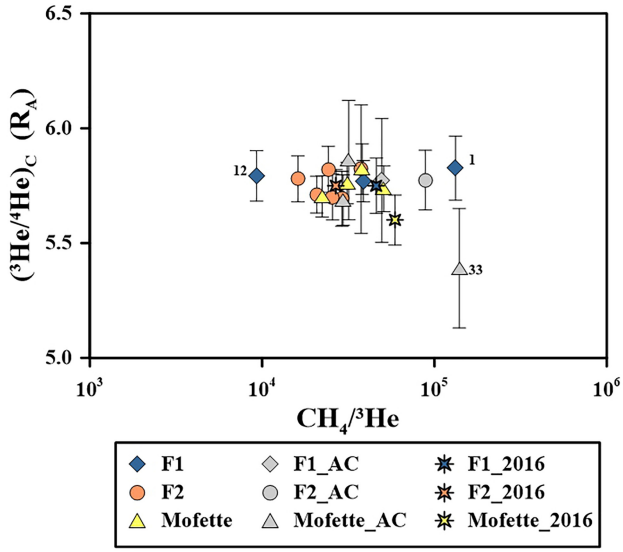

FIGURE 6 | Air-corrected $(^3He/^4He)_c$ vs. $CH_4/^3He$ diagram (cf. Poreda et al., 1988). The abbreviation _AC stands for air contamination, while data of samples collected during 2016 are from Bräuer et al. (2018).

$CH_4/^3He$ ratio may reflect the proportions of crustal and mantle-derived methane (Poreda et al., 1992). In **Figure 6**, the $(^3He/^4He)_c$ ratios are plotted against the $CH_4/^3He$ ratios of the samples collected in the HMF. The values of CH_4 should be considered as minimum estimates, because this gas can be involved in various post-genetic processes, and can also be consumed by methanotrophic bacteria (Murrell and Jetten, 2009; Kip et al., 2012; Gagliano et al., 2020). The $CH_4/^3He$ values range from 1.6×10^4 to 8.9×10^4, with two samples [(1), (33)] that reach up to 1.4×10^5, and one sample [(12)] with only 9.3×10^3. It should be noted that the highest [sample (1)] and the lowest [sample (12)] $CH_4/^3He$ ratios are observed for samples with elevated and depleted CH_4 contents. Likewise, $^3He/^4He$ ratios were relatively constant apart from one sample collected in the mofette during the drilling period [(33), F3 was at ∼197 m depth]. This sample presented a lower isotope ratio, which was most probably due to a higher contribution of crustal He. Except for this single occurrence, no correlation between the $^3He/^4He$ ratios and the drilling depth of F3 was evident.

According to Poreda et al. (1988) and Sakata (1991), low CH_4 contents correspond to low $CH_4/^3He$ ratios in CO_2-rich magmatic gases. This suggests the common origin of CH_4 and He. Mantle-derived fluids typically have $CH_4/^3He$ ratios between 10^5 and 10^8, while those of crust-derived fluids are much higher, and range from 10^8 to 10^{11} (Welhan and Craig, 1979; Giggenbach et al., 1993; Dai et al., 2005). The $CH_4/^3He$ ratios for most of the gases collected in the HMF are lower than 10^5 (**Figure 6**). This indicates that CH_4 may be of volcanic/geothermal origin (Etiope, 2015). If this is the case, CH_4 may have been generated from mantle- and limestone-derived CO_2 or from either of them, according to chemical reactions like Fischer-Tropsch type (FTT) reactions:

$$nCO + (2n + 1)H_2 = C_nH_{2n+2} + nH_2O \quad (2)$$

(Craig, 1953; Berndt et al., 1996; Horita and Berndt, 1999; McCollom and Seewald, 2001), and in the presence of Fe-bearing phase catalysts:

$$CO_2 + 8(FeO) + 2H_2O = CH_4 + 8(FeO_{1.5}) \quad (3)$$

Here FeO and $FeO_{1.5}$ represent iron in the two oxidation states that are generally present in minerals of crustal rocks (Giggenbach, 1987). Both the FTT reactions and the presence of Fe-bearing phase catalysts are fundamental conditions for the chemical and isotope exchange between CO_2 and CH_4 and the establishment of an equilibrium.

In an attempt to determine the P-T conditions under which the gases were formed, the CO_2/Ar and CH_4/Ar ratios were used as geoindicators (**Figure 7**). **Figure 7** was constructed assuming fugacities of H_2O and CO_2 as described in Chiodini et al. (2007). Redox conditions were defined according to D'Amore and Panichi (1980). Excluding the samples affected by air contamination, most samples cluster at T from ∼100 to ∼120^{o}C and P_{CO2} from ∼30 to ∼70 bar. These values can be considered as medium to low P-T conditions that promote the generation of thermogenic CH_4 (Hunt, 1996). Some samples [10), (13), (17), (26), (30), (54)] are characterized by even lower P-T conditions, indicating that the impact of the atmospheric end-member is not negligible in this case. The elevated heat flow values (70–80 mW/m^2, locally as high as 90 mW/m^2; Čermák, 1994) recognized in the area may have contributed to the depleted light hydrocarbon content. It is worth noting that

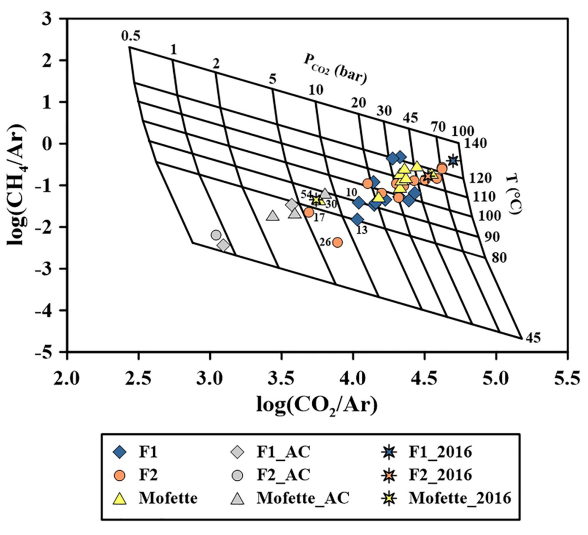

FIGURE 7 | Plot of log(CH_4/Ar) vs. log(CO_2/Ar) after Chiodini et al. (2007). The theoretical P_{CO2}-T grids assume that the redox conditions are fixed by the D'Amore and Panichi (1980) buffer. The abbreviation _AC stands for air contamination, while data of samples collected during 2016 are from Bräuer et al. (2018).

the majority of the gases have values of $CH_4/(C_2H_6+C_3H_8)$ (Bernard ratio; Bernard et al., 1978) in the range of 9 to 93. According to Bernard et al. (1978), these ratios characterize gases of thermogenic origin that are produced by decay of organic matter. If this applies to the gases of the HMF, samples (1), (6), (18), (22), (23), (24), (25), (38), and (39) with Bernard ratios between 100 and 1,000 may reflect secondary processes that stem from inorganic or organic oxidation of CH_4 or mixing of microbial and thermogenic CH_4. Methanogenic archaea detected in various mofette waters in the Cheb Basin (Krauze et al., 2017) may support a biogenic origin of at least parts of the CH_4 present. Moreover, Liu et al. (2018) suggested that the anaerobic and acidophilic taxa identified in soils and sediments collected from two 3-m cores in the HMF may perform methanogenesis under reducing conditions.

Both scenarios seem plausible, however, we cannot confirm or dismiss either of them because the rather low CH_4 concentrations (**Table 1**) did not allow the determination of $\delta^{13}C_{CH4}$ and $\delta^{2}H_{CH4}$ values. Thus, any conclusion on the origin of the gas may be misleading. However, the extraordinary low $CH_4/^3He$ ratios may point to a limited presence of organic matter in the overall process of CH_4 formation. Together with the medium to low P-T conditions, it can be hypothesized that CH_4 in the HMF originates from mixing of volcanic/geothermal and biogenic CH_4 with a non-negligible atmospheric contribution. This hypothesis seems plausible based on the sedimentary formations that characterize the HMF, together with its elevated heat flow values (Čermák, 1994), and the mantle-derived He and CO_2 (Weinlich et al., 1999; Kämpf et al., 2013; Bräuer et al., 2018; this study **Tables 2**, **3**). Procesi et al. (2019) summarized that these are some of the criteria that describe sediment-hosted geothermal systems. Such hybrid geological systems exhibit both volcano-hydrothermal and sedimentary features, in which geothermal and sedimentary domains interact and yield mixtures of inorganic and biogenic gases.

CONCLUSION

The present study investigated processes that affected gases of the HMF in a period when a third borehole was drilled, and no seismic event took place. Changes in CO_2 concentrations are mainly attributed to different solubilities of the gases. This was combined with dilution caused by an enhanced content of atmospheric components. Perturbations on the gas flows, dissolution, and likely FTT reactions had effects on the isotope compositions of CO_2. Moreover, data from the wellhead pressure of F2 as well as from the gas flow of F1 support the assumption that the boreholes are hydraulically connected.

Variations in CH_4 contents indicated generation and consumption of this gas. Despite the lack of CH_4 isotope data, we suggest that CH_4 may be of mixed biogenic and volcanic/geothermal origin. In any case, it derives from sediments characterized by medium to low P-T conditions. It is unclear if it is solely derived from the mantle or also influenced by limestone-derived CO_2 under conditions in which FTT reactions and Fe catalysts are present. The drilling of the third borehole highlighted the complexity of the HMF in a seismically quiescent period. It opens the opportunity for further geochemical investigations in the area.

DATA AVAILABILITY STATEMENT

The original contributions presented in the study are included in the article/**Supplementary Materials**, further inquiries can be directed to the corresponding author.

AUTHOR CONTRIBUTIONS

HW, MZ, SN, and JB developed the conception and design of the MoRe project. KD was responsible for the gas sampling, while all the authors assisted in the field campaigns. AV-H was responsible for the $\delta^{13}C_{CO2}$ analyses, while SN was responsible for the noble gas analyses. JV was responsible for the gas flow, pressure, and temperature measurements. KD wrote the first draft of the manuscript. All authors contributed to manuscript revision, read and approved the submitted version.

FUNDING

This research was a part of the MoRe – "Mofette Research" project, which is included in the International Continental Scientific Drilling Program (ICDP) project "Drilling the Eger Rift: Magmatic fluids driving the earthquake swarms and the deep biosphere." This work was funded by the Deutsche Forschungsgemeinschaft (DFG, German Research Foundation) – 419880416.

ACKNOWLEDGMENTS

We would like to thank Walter D'Alessandro and Artur Ionescu for the fruitful discussions during the preparation of this manuscript. We are indebted to all the laboratory technicians for performing the various analyses: Enzio Schnabel (noble gas measurements), Doreen Noack (carbon isotopes), and Jiři Tesař (chemical composition). We also thank Pouria Marzban for sharing the orthomosaic image presented in **Figure 1**. We are also grateful for the insightful comments of the two reviewers and of the editor YW that helped us to significantly improve the manuscript.

SUPPLEMENTARY MATERIAL

The Supplementary Material for this article can be found online at: https://www.frontiersin.org/articles/10.3389/feart.2021.615766/full#supplementary-material

REFERENCES

Babuška, V., and Plomerová, J. (2008). Control of paths of quaternary volcanic products in western bohemian massif by rejuvenated variscan triple junction of ancient microplates. *Stud. Geophys. Geod.* 52, 607–629. doi: 10.1007/s11200-008-0040-0

Bankwitz, P., Schneider, G., Kämpf, H., and Bankwitz, E. (2003). Structural characteristics of epicentral areas in Central Europe: study case cheb basin (Czech Republic). *J. Geodyn.* 35, 5–32. doi: 10.1016/s0264-3707(02)00051-0

Bernard, B. B., Brooks, J. M., and Sackett, W. M. (1978). *A Geochemical Model for Characterization of Hydrocarbon gas Sources in Marine Sediments*. Houston, TX: Offshore Technology Conference, 435–438.

Berndt, M. E., Allen, D. E., and Seyfried, W. E. (1996). Reduction of CO_2 during serpentinization of olivine at 300°C and 500 bar. *Geology* 24, 351–354. doi: 10.1130/0091-7613(1996)024<0351:rocdso>2.3.co;2

Bottinga, Y. (1968). Calculation of fractionation factors for carbon and oxygen isotopic exchange in the system calcite–carbon dioxide–water. *J. Phys. Chem.* 72, 800–808. doi: 10.1021/j100849a008

Bräuer, K., Kämpf, H., Niedermann, S., and Strauch, G. (2005). Evidence for ascending upper mantle-derived melt beneath the Cheb basin, Central Europe. *Geophys. Res. Lett.* 32:L08303. doi: 10.1029/2004GL022205

Bräuer, K., Kämpf, H., Niedermann, S., and Strauch, G. (2018). Monitoring of helium and carbon isotopes in the western Eger Rift area (Czech Republic): relationships with the 2014 seismic activity and indications for recent (2000–2016) magmatic unrest. *Chem. Geol.* 482, 131–145. doi: 10.1016/j.chemgeo.2018.02.017

Bräuer, K., Kämpf, H., and Strauch, G. (2009). Earthquake swarms in non-volcanic regions: what fluids have to say. *Geophys. Res. Lett.* 36:L17309. doi: 10.1029/2009GL039615

Bussert, R., Kämpf, H., Flechsig, C., Hesse, K., Nickschick, T., Liu, Q., et al. (2017). Drilling into an active mofette: pilot-hole study of the impact of CO_2-rich mantle-derived fluids on the geo–bio interaction in the western Eger Rift (Czech Republic). *Sci. Dril.* 23, 13–27. doi: 10.5194/sd-23-13-2017

Čermák, V. (1994). "Results of heat flow studies in Czechoslovakia, in crustal structure of the bohemian massif and the west carpathians," in *Exploration of the Deep Continental Crust*, eds V. Bucha and M. Blížkovs.ký (Berlin: Springer-Verlag), 85–120. doi: 10.1007/978-3-642-78995-3_4

Chiodini, G., Baldini, A., Barberi, F., Carapezza, M. L., Cardellini, C., Frondini, F., et al. (2007). Carbon dioxide degassing at Latera caldera (Italy): evidence of geothermal reservoir and evaluation of its potential energy. *J. Geophys. Res.* 112:B12204. doi: 10.1029/2006JB004896

Chiodini, G., Cardellini, C., Caliro, S., Chiarabba, C., and Frondini, F. (2013). Advective heat transport associated with regional earth degassing incentral apennine (Italy). *Earth Planet. Sci. Lett.* 373, 65–74. doi: 10.1016/j.epsl.2013.04.009

Chiodini, G., Frondini, F., Cardellini, C., Parello, F., and Peruzzi, L. (2000). Rate of diffuse carbon dioxide earth degassing estimated from carbon balance of regional aquifers: the case of central Apennine, Italy. *J. Geophys. Res.* 105, 8423–8434. doi: 10.1029/1999jb900355

Craig, H. (1953). The geochemistry of the stable carbon isotopes. *Geochim. Cosmochim. Acta.* 3, 53–92. doi: 10.1016/0016-7037(53)90001-5

Craig, H., Lupton, J. E., and Horribe, Y. (1978). A mantle helium component in Circum-Pacific Rise volcanic gases: hakone, the Marianas, and Mt Lassen. *Terr. Rare Gases* 3, 3–16. doi: 10.1007/978-94-010-9828-1_1

Dahm, T., Hrubcová, P., Fischer, T., Horálek, J., Korn, M., Buske, S., et al. (2013). Eger Rift ICDP: an observatory for study of non-volcanic, mid-crustal earthquake swarms and accompanying phenomena. *Sci. Dril.* 16, 93–99. doi: 10.5194/sd-16-93-2013

Dai, J. X., Yang, S. F., Chen, H. L., and Shen, X. H. (2005). Geochemistry and occurrence of inorganic gas accumulations in Chinese sedimentary basins. *Org. Geochem.* 36, 1664–1688. doi: 10.1016/j.orggeochem.2005.08.007

D'Alessandro, W., Brusca, L., Kyriakopoulos, K., Bellomo, S., and Calabrese, S. (2014). A geochemical traverse along the "Sperchios Basin — Evoikos Gulf" Graben (Central Greece): origin and evolution of the emitted fluids. *Mar. Pet. Geol.* 55, 295–308. doi: 10.1016/j.marpetgeo.2013.12.011

D'Alessandro, W., Brusca, L., Martelli, M., Rizzo, A., and Kyriakopoulos, K. (2010). Geochemical characterization of natural gas manifestations in Greece. *Bull. Geol. Soc. Gr.* 43, 2327–2337. doi: 10.12681/bgsg.11633

D'Amore, F., and Panichi, C. (1980). Evaluation of deep temperatures of hydrothermal systems by a new gas geothermometer. *Geochim. Cosmochim. Acta* 44, 549–556. doi: 10.1016/0016-7037(80)90051-4

Daskalopoulou, K., Calabrese, S., Grassa, F., Kyriakopoulos, K., Parello, F., Tassi, F., et al. (2018). Origin of methane and light hydrocarbons in natural fluid emissions: a key study from Greece. *Chem. Geol.* 479, 286–301. doi: 10.1016/j.chemgeo.2018.01.027

Easley, E., Garchar, L., Bennett, M., Morgan, P., and Wendlandt, R. F. (2011). A geochemical and isotopic study of two geothermal prospects in the Rio Grande Rift, Colorado and New Mexico. *Mt. Geol.* 48, 95–106.

Etiope, G. (2015). *Natural Gas Seepage: The Earth's Hydrocarbon Degassing*. Berlin: Springer, 141. doi: 10.1007/978-3-319-14601-0

Fiala, J., and Vejnar, Z. (2004). The lithology, geochemistry, and metamorphic gradation of the crystalline basement of the Cheb (Eger) Tertiary Basin, Saxothuringian Unit. *Bull. Geosci.* 79, 41–52.

Fischer, T., and Horálek, J. (2003). Space-time distribution of earthquake swarms in the principal focal zone of the NW-Bohemian/Vogtland seismoactive region: period 1985-2001. *J. Geodyn.* 35, 125–144. doi: 10.1016/S0264-3707(02)00058-3

Fischer, T., Horálek, J., Hrubcová, P., Vavryčuk, V., Bräuer, K., and Kämpf, H. (2014). Intra-continental earthquake swarms in West-Bohemia and Vogtland: a review. *Tectonophysics* 611, 1–27. doi: 10.1016/j.tecto.2013.11.001

Fischer, T., and Michálek, J. (2008). Post 2000-swarm microearthquake activity in the principal focal zone of West Bohemia/Vogtland: space-time distribution and waveform similarity analysis. *Stud. Geophys. Geod.* 52, 493–511. doi: 10.1007/s11200-008-0034-y

Fischer, T., Matyskac, C., and Heinicke, J. (2017). Earthquake-enhanced permeability – evidence from carbon dioxide release following the M_L 3.5 earthquake in West Bohemia, Earth Planet. *Sc. Lett.* 460, 60–67. doi: 10.1016/j.epsl.2016.12.001

Fischer, T., Vlček, J., and Lanzendörfer, M. (2020). Monitoring crustal CO_2 flow: methods and their applications to the mofettes in West Bohemia. *Solid Earth* 11, 983–998. doi: 10.5194/se-11-983-2020

Fischer, T. P., Giggenbach, W. F., Sano, Y., and Williams, S. N. (1998). Fluxes and sources of volatiles discharged from Kudryavy, a subduction zone volcano, Kurile Islands. *Earth Planet Sci Lett* 160, 81–96. doi: 10.1016/s0012-821x(98)00086-7

Foustoukos, D. I., and Seyfried, W. E. (2004). Hydrocarbons in hydrothermal vent fluids: the role of chromium-bearing catalysts. *Science* 304, 1002–1004. doi: 10.1126/science.1096033

Gagliano, A. L., Calabrese, S., Daskalopoulou, K., Kyriakopoulos, K., Tagliavia, M., and D'Alessandro, W. (2020). Methanotrophy in geothermal soils, an overlooked process: the example of Nisyros island (Greece). *Chem. Geol.* 539:119546. doi: 10.1016/j.chemgeo.2020.119546

Geissler, W. H., Kämpf, H., Kind, R., Klinge, K., Plenefisch, T., Horálek, J., et al. (2005). Seismic structure and location of a CO_2 source in the upper mantle of the western Eger (Ohře) Rift, Central Europe. *Tectonics* 24:TC5001. doi: 10.1029/2004TC001672

Giggenbach, W. F. (1987). Redox processes governing the chemistry of fumarolic gas discharges from White Island, New Zealand. *Appl. Geochem.* 2, 143–161. doi: 10.1016/0883-2927(87)90030-8

Giggenbach, W. F. (1992). The composition of gases in geothermal and volcanic systems as a function of tectonic setting. *Water Rock Interact.* 2, 873–878.

Giggenbach, W. F. (1996). "Chemical composition of volcanic gases," in *Monitoring and Mitigation of Volcano Hazards*, eds R. Scarpa and R. I. Tilling (Berlin: Springer), 221–256. doi: 10.1007/978-3-642-80087-0_7

Giggenbach, W. F., Gonfianti, R., Jangi, B. L., and Truesdell, A. H. (1983). Isotopic and chemical composition of Parbati Valley geothermal discharges, North-West Himalaya, India. *Geothermics* 12, 199–222. doi: 10.1016/0375-6505(83)90030-5

Giggenbach, W. F., Sano, Y., and Wakita, H. (1993). Isotopic composition of helium, and CO_2 and CH_4 contents in gases produced along the New Zealand part of a convergent plate boundary. *Geochim. Cosmochim. Acta* 57, 3427–3455. doi: 10.1016/0016-7037(93)90549-c

Goff, F., and Janik, C. J. (2002). Gas geochemistry of the Valles caldera region, New Mexico and comparisons with gases at Yellowstone, Long Valley and other geothermal systems. *J. Volcanol. Geotherm. Res.* 116, 299–323. doi: 10.1016/s0377-0273(02)00222-6

Heaton, T. H. E., and Vogel, J. C. (1981). Excess air in groundwater. *J. Hydrol.* 50, 201–208. doi: 10.1016/0022-1694(81)90070-6

Hecht, L., Vigneresse, J., and Morteani, G. (1997). Constraints on the origin of zonation of the granite complexes in the Fichtelgebirge (Germany and Czech Republic): evidence from a gravity and geochemical study. *Geol. Rundsch.* 86, S93–S109.

Hickman, S., Sibson, R., and Bruhn, R. (1995). Introduction to special section: mechanical involvement of fluids in faulting. *J. Geophys. Res.* 100, 12831–12840. doi: 10.1029/95jb01121

Horita, J., and Berndt, M. E. (1999). Abiogenic methane formation and isotopic fractionation under hydrothermal conditions. *Science* 285, 1055–1057. doi: 10.1126/science.285.5430.1055

Hunt, J. M. (1996). *Petroleum Geochemistry and Geology*. New York, NY: W.H. Freeman and Co, 743.

Irwin, W. P., and Barnes, I. (1980). Tectonic relations of carbon dioxide discharges and earthquakes. *J. Geophys. Res.* 85, 3115–3121. doi: 10.1029/jb085ib06p03115

Italiano, F., De Santis, A., Favali, P., Rainone, M. L., Ruisi, S., and Signanini, S. (2014a). The marsili volcanic seamount (Southern Tyrrhenian Sea): a potential offshore geothermal resource. *Energies* 7, 4068–4086. doi: 10.3390/en7074068

Italiano, F., Kis, B. M., Baciu, C., Ionescu, A., Harangi, S., and Palcsu, L. (2017). Geochemistry of dissolved gases from the eastern carpathians – transylvanian basin boundary. *Chem. Geol.* 469, 117–128. doi: 10.1016/j.chemgeo.2016.12.019

Italiano, F., Yuce, G., Uysal, I. T., Gasparon, M., and Morelli, G. (2014b). Insights into mantle type volatiles contribution from the dissolved gases in artesian waters of the Great Artesian Basin, Australia. *Chem. Geol.* 378-379, 75–88. doi: 10.1016/j.chemgeo.2014.04.013

Kämpf, H., Bräuer, K., Schumann, J., Hahne, K., and Strauch, G. (2013). CO_2 discharge in an active, non-volcanic continental rift area (Czech Republic): characterisation ($\delta^{13}C$, $^3He/^4He$) and quantification of diffuse and vent CO_2 emissions. *Chem. Geol.* 339, 71–83. doi: 10.1016/j.chemgeo.2012.08.005

Kämpf, H., Broge, A. S., Marzban, P., Allahbakhshi, M., and Nickschick, T. (2019). Nonvolcanic carbon dioxide emission at continental rifts: the bublak mofette area, western eger rift, czech republic. *Geofluids* 2019:4852706. doi: 10.1155/2019/4852706

Kip, N., Fritz, C., Langelaan, E. S., Pan, Y., Bodrossy, L., Pancotto, V., et al. (2012). Methanotrophic activity and diversity in different *Sphagnum magellanicum* dominated habitats in the southernmost peat bogs of Patagonia. *Biogeosciences* 9, 47–55. doi: 10.5194/bg-9-47-2012

Krauze, P., Kämpf, H., Horn, F., Liu, Q., Voropaev, A., Wagner, D., et al. (2017). Microbiological and geochemical survey of CO_2-dominated mofette and mineral waters of the Cheb Basin, Czech Republic. *Front. Microbiol.* 8:2446. doi: 10.3389/fmicb.2017.02446

Lee, H., Yang, T. F., Lan, T. F., Song, S., and Tsao, S. (2005). Fumarolic gas composition of the Tatun Volcano Group, northern Taiwan. *Terr. Atmos. Ocean Sci.* 16, 843–864. doi: 10.3319/tao.2005.16.4.843(gig)

Liu, Q., Kämpf, H., Bussert, R., Krauze, P., Horn, F., Nickschick, T., et al. (2018). Influence of CO_2 degassing on the microbial community in a dry mofette field in Hartoušov, Czech Republic (Western Eger Rift). *Front. Microbiol.* 9:2787. doi: 10.3389/fmicb.2018.02787

Lupton, J. E. (1983). Terrestrial inert gases: isotope tracer studies and clues to primordial components in the mantle. *Annu. Rev. Earth Planet. Sci.* 11, 371–414. doi: 10.1146/annurev.ea.11.050183.002103

McCollom, T. M., and Seewald, J. S. (2001). A reassessment of the potential for reduction of dissolved CO_2 to hydrocarbons during serpentinization of olivine. *Geochim. Cosmochim. Acta.* 65, 3769–3778. doi: 10.1016/s0016-7037(01)00655-x

Mrlina, J., Kämpf, H., Kroner, C., Mingram, J., Stebich, M., Brauer, A., et al. (2009). Discovery of the first quaternary maar in the Bohemian Massif, central Europe, based on combined geophysical and geological surveys. *J. Volcanol. Geotherm. Res.* 182, 97–112. doi: 10.1016/j.jvolgeores.2009.01.027

Murrell, C. J., and Jetten, M. S. M. (2009). The microbial methane cycle. *Environ. Microbiol. Reports* 1, 279–284. doi: 10.1111/j.1758-2229.2009.00089.x

Nickschick, T., Kämpf, H., Flechsig, C., Mrlina, J., and Heinicke, J. (2015). CO_2 degassing in the Hartoušov mofette area, western Eger Rift, imaged by CO_2 mapping and geoelectrical and gravity surveys. *Int. J. Earth Sci.* 104, 2107–2129. doi: 10.1007/s00531-014-1140-4

Niedermann, S., Bach, W., and Erzinger, J. (1997). Noble gas evidence for a lower mantle component in MORBs from the southern East Pacific rise: decoupling of helium and neon isotope systematics. *Geochim. Cosmochim. Acta* 61, 2697–2715. doi: 10.1016/s0016-7037(97)00102-6

Parotidis, M., Rothert, R., and Shapiro, S. A. (2003). Pore-pressure diffusion: a possible triggering mechanism for the earthquake swarms 2000 in the Vogtland/NW Bohemia, central Europe. *Geophys. Res. Lett.* 30, 2075. doi: 10.1029/2003GL018110

Pearce, J. M., Czernichowski-Lauriol, I., Lombardi, S., Brune, S., Mador, A., Baker, J., et al. (2004). "A review of natural CO_2 accumulations in Europe as analogues for geological sequestration," in *Geological Storage of Carbon Dioxide*, Vol. 233, eds S. Baines and R.H. Worden (London: Geological Society of London), 29–42. doi: 10.1144/GSL.SP.2004.233.01.04

Poreda, R. J., Craig, H., Arnórsson, S., and Welhan, J. A. (1992). Helium isotopes in Icelandic geothermal systems: I. ^3He, gas chemistry, and ^{13}C relations. *Geochim. Cosmochim. Acta* 56, 4221–4228. doi: 10.1016/0016-7037(92)90262-H

Poreda, R. J., Jeffrey, A. W., Kaplan, I. R., and Craig, H. (1988). Magmatic helium in subduction zone natural gases. *Chem. Geol.* 71, 198–210.

Procesi, M., Ciotoli, G., Mazzini, A., and Etiope, G. (2019). Sediment-hosted geothermal systems: review and first global mapping. *Earth Sci. Rev.* 192, 529–544. doi: 10.1016/j.earscirev.2019.03.020

Ray, M. C., Hilton, D. R., Munoz, J., Fischer, T. P., and Shaw, A. M. (2009). The effects of volatile recycling, degassing and crustal contamination on helium and carbon geochemistry of hydrothermal fluids from the Southern Volcanic Zone of Chile. *Chem. Geol.* 266, 38–49. doi: 10.1016/j.chemgeo.2008.12.026

Reid, R. C., Prausnitz, J. M, and Poling, B. E. (1987). *The Properties of Gases and Liquids*. New York, NY: McGraw-Hill, Inc.

Ring, U., Uysal, I. T., Yüce, G., Ünal-Ýmer, E., Italiano, F., Ýmer, A., et al. (2016). Recent mantle degassing recorded in carbonic spring deposits along sinistral strike-slip faults, south central Australia. *Earth Planet. Sci. Lett.* 454, 304–318. doi: 10.1016/j.epsl.2016.09.017

Rolston, D. E., Duxbury, J. M., Harper, L. A., Mosier, A. R., and Knowles, R. (1993). *Methane: Processes of Production and Consumption. ASA Special Publication*. Madison, WI: American Society of Agronomy, doi: 10.2134/asaspecpub55.c10

Sakata, S. (1991). Carbon isotope geochemistry of natural gases from the Green Tuff Basin, Japan. *Geochim. Cosmochim. Acta* 55, 1395–1405. doi: 10.1016/0016-7037(91)90316-w

Špičáková, L., Uličný, D., and Koudelková, G. (2000). Tectonosedimentary evolution of the Cheb Basin (NW Bohemia, Czech Republic) between Late Oligocene and Pliocene: a preliminary note. *Stud. Geophys. Geod.* 44, 556–580.

Weinlich, F. H., Bräuer, K., Kämpf, H., Strauch, G., Tesař, J., and Weise, S. M. (1999). An active subcontinental mantle volatile system in the western Eger rift, Central Europe: Gas flux, isotopic (He, C, and N) and compositional fingerprints. *Geochim. Cosmochim. Acta* 63, 3653–3671. doi: 10.1016/s0016-7037(99)00187-8

Weinlich, F. H., Tesař, J., Weise, S. M., Bräuer, K., and Kämpf, H. (1998). Gas flux distribution in mineral springs and tectonic structure in the western Eger Rift. *J. Czech Geol. Soc.* 43, 91–110.

Weise, S. M., Bräuer, K., Kämpf, H., Strauch, G., and Koch, U. (2001). Transport of mantle volatiles through the crust traced by seismically released fluids: a natural experiment in the earthquake swarm area Vogtland/NW Bohemia, central Europe. *Tectonophysics* 336, 137–150. doi: 10.1016/s0040-1951(01)00098-1

Welhan, J. A., and Craig, H. (1979). Methane and hydrogen in East Pacific rise hydrothermal fluids. *Geophys. Res. Lett.* 6, 829–832. doi: 10.1029/gl006i011p00829

Welhan, J. A., and Craig, H. (1983). "Methane, hydrogen and helium in hydrothermal fluids," in *Hydrothermal Processes at Seafloor Spreading Centers*, Vol. 12, eds P. A. Rona, K. Boström, L. Laubier, and K. L. Smith (Boston, MA: Plenum Press), 39l–409l.

Woith, H., Daskalopoulou, K., Zimmer, M., Fischer, T., Vlček, J., Trubač, J., et al. (2020). Multi-level gas monitoring: a new approach in earthquake research. *Front. Earth Sci.* 8:585733. doi: 10.3389/feart.2020.585733

Yuce, G., Italiano, F., D'Alessandro, W., Yalcin, T. H., Yasin, D. U., Gulbay, A. H., et al. (2014). Origin and interactions of fluids circulating over the Amik Basin (Hatay-Turkey) and relationships with the hydrologic, geologic and tectonic settings. *Chem. Geol.* 388, 23–39. doi: 10.1016/j.chemgeo.2014.09.006

Conflict of Interest: The authors declare that the research was conducted in the absence of any commercial or financial relationships that could be construed as a potential conflict of interest.